PAPER

Check for updates

Highly efficient removal of Sr^{2+} from aqueous solutions using a polyacrylic acid/crown-ether/graphene oxide hydrogel composite

Sheng Chen,[ab] Lina Wu, [ID] [b] Zhicheng Wu,*[b] Zhikun Liu,[b] Zhihua Qiu[b] and Lisheng Chi [ID] *[b]

With the development of nuclear power, efficiently treating nuclear wastes generated during operation has attracted extensive attention. Hydrogels are common adsorbent materials in the treatment of wastewater due to their high swelling rate and easy post-treatment. In this work, a novel polyacrylic acid/crown-ether/graphene oxide (PAA/DB18C6/GO) hydrogel composite was synthesized by a radical cross-linking copolymerization method and characterized using various analytical tools such as SEM, FT-IR, TGA and XPS. The effects of time, pH, initial Sr^{2+} concentration, and temperature on Sr^{2+} adsorption onto the PAA/DB18C6/GO were studied. The PAA/DB18C6/GO shows a high adsorption capacity of 379.35 mg g^{-1} at an initial Sr^{2+} concentration of 772 mg L^{-1} due to the unique structure of dibenzo-18-crown-ether-6 and high swelling. The composite has a high selectivity for Sr^{2+} with a removal rate of 82.4% when concentrations of Na$^+$ and K$^+$ were 10 times higher than that of Sr^{2+}. The pH and temperature have no apparent impact on adsorption performance of the PAA/DB18C6/GO under the experimental conditions. The composite shows excellent reusability with more than 92% removal rate for Sr^{2+} after five continuous cycles. In addition, the mechanism of Sr^{2+} adsorption by PAA/DB18C6/GO was analyzed by fitting the adsorption data to the theoretical models and XPS data.

1 Introduction

Nuclear power as a clean energy is recently attracting more attention worldwide to reduce greenhouse gas emission and to mitigate greenhouse effects.[1,2] However, disposing of nuclear wastes generated during operation remains challenging.[3] Sr-90 with a half-life of 28.8 years is one of the highly radioactive nuclides present in high-level radioactivity nuclear wastes.[4,5] Strontium is an alkaline earth metal with properties similar to those of calcium. Once Sr-90 is released into the environment, it easily enters the human body through the food chain and accumulates in the bones, which will continuously harm the person's health.[6,7] Therefore, it is important to develop an effective material that can efficiently remove Sr-90 from radioactive wastes.

Many methods have been attempted to remove strontium ions from solution, such as chemical precipitation,[8] solvent extraction,[9,10] membrane separation[11,12] and adsorption.[13,14] Compared to other methods, adsorption method has a number of advantages, such as simple operation, high removal efficiency and large treatment capacity.[13,15] A variety of strontium adsorption materials have been so far developed, including zeolites,[16] graphene,[12] silica-titanates,[17,18] sulfides,[19] metal–organic frameworks,[20] and polymers.[21] Hydrogel as a common adsorbent has attracted lots of attention because of its low cost, easy operation and high adsorption capacity.[22] Polyacrylic acid (PAA) can be prepared as a hydrogel with good adsorption properties due to the large number of carboxylic acid groups on the surfaces, so it could be widely used for the treatment of liquid wastes.[23] In addition, hydrogel adsorbents generally have high swelling rate which increases the contact area with the solution and can effectively promote the adsorption. Therefore, polymeric hydrogels usually have good adsorption capacity and regeneration performance under wide pH conditions.[24] The PAA-based hydrogel materials have been studied for the removal of metal ions.[25,26]

Among Sr^{2+} adsorption materials, crown-ether is one of the most studied materials due to its unique structure and high selectivity for Sr^{2+}.[27] Crown-ether is a macrocyclic compound that can form strong complexes with alkali metals or alkaline earth metals *via* strong complexation force.[28,29] It was found that 18-crown-ether-6 and its derivatives are the most effective adsorbents in removing Sr^{2+} as their pore size is in the range 0.26–0.32 nm that is suited to ingress of strontium ion.[27,30] Therefore, dibenzo-18-crown-ether-6 (DB18C6) has been used as a filler in the polymer composite to enhance its selectivity for Sr^{2+}.[31] Meanwhile graphite oxide (GO) has been reported as an

[a]*College of Chemistry, Fuzhou University, Fuzhou, Fujian 350108, China*

[b]*Fujian Key Laboratory of Fuel and Materials in Clean Nuclear Energy System, Fujian Institute of Research on the Structure of Matter, CAS, Fuzhou, Fujian 350002, China. E-mail: lchi@fjirsm.ac.cn*

efficient adsorbent due to its high content of oxygen-containing functional groups, including carboxyl, hydroxyl and epoxy groups.[32,33] In recent years, graphene oxide has been frequently added to polymeric adsorbents to improve the network structure and adsorption properties.[23,34,35]

As crown-ether has a unique heterocyclic structure, if it could be compounded with PAA and GO, the composite would not only have the suitable pore size for selectively capturing Sr^{2+}, but also contain large number of carboxyl and hydroxyl groups which can increase its adsorption capacity. Therefore, the composite adsorbent could be a highly efficient material for treating of radioactive wastes containing strontium radionuclides. As a result, in this work, the polyacrylic acid/crown-ether/graphene oxide hydrogel composites (PAA/DB18C6/GO) were explored and successfully synthesized by free-radical cross-linking copolymerization of acrylic acid (AA) monomer in deionized water using N,N'-methylenebis acrylamide (MBA) as a cross-linker and potassium persulfate (KPS) as an initiator with dibenzo-18-crown-ether-6 (DB18C6) and graphene oxide (GO) as filler. The effects of environmental factors including contact time, pH, initial Sr^{2+} concentration and temperature on the adsorption performance of PAA/DB18C6/GO were investigated in details to evaluate its adsorption capacity and suitability. In addition, desorption and regeneration experiments were conducted to study its reusability. The adsorption behavior of Sr^{2+} was analyzed by adsorption kinetic model and adsorption isotherm model. All the results suggest that the PAA/DB18C6/GO could be a prospective adsorbent material for the removal of Sr^{2+} from high level radioactivity liquid waste.

2 Experimental

2.1 Material

Acrylic acid ($CH_2CHCOOH$, 99%) was purchased from Shanghai Macklin Biochemical Technology Company. Potassium persulfate ($K_2S_2O_8$, 99.5%), strontium nitrate ($Sr(NO_3)_2$, 99%), sodium nitrate ($NaNO_3$, 99%), potassium nitrate (KNO_3, 99%) and ethylenediaminetetraacetic acid disodium salt dihydrate ($C_{10}H_{14}N_2Na_2O_8 \cdot 2H_2O$, EDTA-2Na, 99%) were purchased from Shanghai Sinopharm Chemical Reagent Company. Dibenzo-18-crown-ether-6 ($C_{20}H_{24}O_6$, 98%), diaminodibenzo-18-crown-6 ($C_{20}H_{28}O_6N_2$), N,N'-methylenebis acrylamide ($C_7H_{10}N_2O_2$, 99%), sodium hydroxide (NaOH, 96%) were obtained from Shanghai Aladdin Biochemical Technology Company. Graphene oxide (C, 97% peelable rate) was obtained from China Graphene Research Institute. The acrylic acid was purified by vacuum distillation prior to the experiments, while the other chemicals were used as received without further purification. Water used in the experiments was provided by the ultra-pure water purification equipment (Direct-Q5UV Millipore, 18.2 MΩ cm @ 25 °C).

2.2 Characterization

Morphology and microstructure of the adsorbents before and after adsorption were characterized using the Hitachi SU8010 field emission scanning electron microscope (SEM). The Fourier transform infrared spectroscopy (FT-IR) spectra were collected on a Bruker Optics Vertex 70 infrared spectrometer in a scan range from 400 cm^{-1} to 4000 cm^{-1}. Thermogravimetric analysis (TGA) was conducted using a Netzsch STA 499F3 type thermal analyzer in the temperature range from 30 °C to 800 °C under a nitrogen gas flow to determine thermal stability of the samples. The elemental composition and electron binding energies of the composites were characterized by X-ray photoelectron spectroscopy (XPS) and obtained on a Thermo Fisher Escalab 250Xi X-ray photoelectron spectrometer. The ion concentrations in the solutions were measured using the PerkinElmer Avio 200 inductively coupled plasma optical emission spectrometry (ICP-OES).

2.3 Preparation of PAA/DB18C6/GO hydrogel composite

54 mg of DB18C6 was added to 3.6 g of AA monomer under stirring until completely dissolved. The solution was diluted using the ultrapure water to obtain the monomer concentration of 55% in weight, followed by adding an amount of sodium hydroxide solution (20 wt%) under ice bath conditions to neutralize the solution. 10 mg of graphene oxide powder and 28.8 mg of MBA were added to the solution that was transferred to a three-neck flask. Then the flask was evacuated, followed by bubbling with nitrogen gas to remove the air. After the solution was heated to 45 °C, 21.6 mg of KPS was added to start polymerization reaction until the solution became a hydrogel state. The product was soaked and washed with ultrapure water to remove the unreacted reactants, followed by drying in a freeze-dryer for 3 days. The dried product (PAA/DB18C6/GO) was crushed into pellets using a grinder for adsorption experiments. The pure PAA hydrogels were also synthesized using the similar method.

2.4 Absorbency experiments

The absorbency experiments were carried out to investigate the water absorption capacity of the hydrogel composite. The 10 mg dried hydrogel samples were immersed in a sufficient amount of deionized water at room temperature for 48 h to examine swelling equilibrium of the hydrogel composites.

Swelling rate (SR) of the hydrogel composite can be calculated using the following eqn (1):

$$SR = \frac{W_s - W_0}{W_0} \tag{1}$$

where W_0 (mg) and W_s (mg) are weights of the hydrogel samples in the original dried state and the swollen state, respectively.

2.5 Batch adsorption experiments

Batch adsorption experiments of Sr^{2+} on the PAA/DB18C6/GO and PAA hydrogel composites were performed in polyethylene centrifuge tubes. 20 mg of adsorbent was added to 20 ml of the Sr^{2+} solution, followed by shaking in an oscillator for 300 min when the adsorption equilibrium had been reached. The adsorbent was removed with an injection filter and the concentration of Sr^{2+} in the solution before and after adsorption was measured using ICP-OES.

In this study, the effects of pH, temperature, competing ions, and Sr^{2+} concentration on the adsorption performance of PAA/DB18C6/GO and PAA were carried out. In addition, desorption experiments of Sr^{2+} adsorbed on PAA/DB18C6/GO were investigated using 0.12 mol per L EDTA-2Na solution. After each desorption, the hydrogels were washed again with 1 mol per L NaOH and deionized water, respectively. After regeneration, the adsorption experiments of the PAA and PAA/DB18C6/GO hydrogels were repeated under the same conditions for five consecutive cycles in terms of adsorption and regeneration.

The equilibrium adsorption capacity (Q_e, mg g^{-1}) and adsorption efficiency (R, %) were used to evaluate the adsorption performance of the adsorbents, as shown in the following eqn (2) and (3):

$$Q_e = \frac{(C_0 - C_e)/V}{m} \qquad (2)$$

$$R = \frac{C_0 - C_e}{C_0} \times 100\% \qquad (3)$$

where C_0 (mg L^{-1}) and C_e (mg L^{-1}) are the concentration of Sr^{2+} in the solution at the initial and equilibrium adsorption, respectively; V (ml) is the volume of the Sr^{2+} solution; m (mg) is the mass of the adsorbent used.

3 Results and discussion

3.1 Structural characterizations

3.1.1 SEM morphology analysis. The morphology images of the PAA and PAA/DB18C6/GO were obtained by scanning electron microscopy as shown in Fig. 1. A uniform network structure with a number of pores can be clearly observed in the PAA hydrogel in Fig. 1(a), which is considered to be macro porous hydrogel due to the pore diameter in the range 0.1–1 μm.[26,36,69,70] Pores in the hydrogel facilitate diffusion of the solution and improve absorbent properties with fast swelling kinetics.[37] The PAA/DB18C6/GO hydrogel composite in Fig. 1(b) also shows

similar network structure and pores, while the surface with numerous clavicle-shaped dibenzo-18-crown-ether-6 particles is rougher than the PAA.[38] The rough surface and pores of the material improve contact of the hydrogel with the solution, while the network structure maintains the basic properties of the hydrogel even after water absorption.[24]

3.1.2 FT-IR analysis. The chemical components and functional groups of PAA and PAA/DB18C6/GO were characterized by FT-IR spectra, as shown in Fig. 2. On the FT-IR spectra of PAA, the 1706 cm^{-1} peak is ascribed to the stretching vibration of C=O in the –COOH function group and the 1448 cm^{-1} peak to the stretching vibration of –CH$_2$,[39,40] while the wide peak at 3647 cm^{-1} corresponds to the stretching vibration of the –OH group. As can be seen from the FT-IR of PAA/DB18C6/GO, the peak at 2949 cm^{-1} is assigned to the stretching vibration of the –CH$_2$ group in the crown ether, while the 1685 cm^{-1} and 1406 cm^{-1} peaks arise from the antisymmetric and symmetric stretching vibrations of the –COO$^-$ group, respectively. Meanwhile the peak at 1558 cm^{-1} is attributed to the skeletal
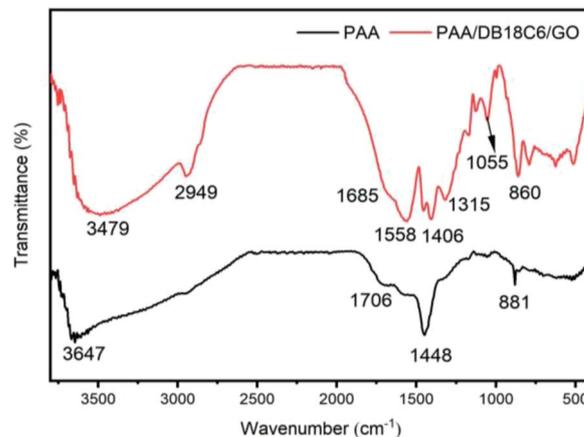

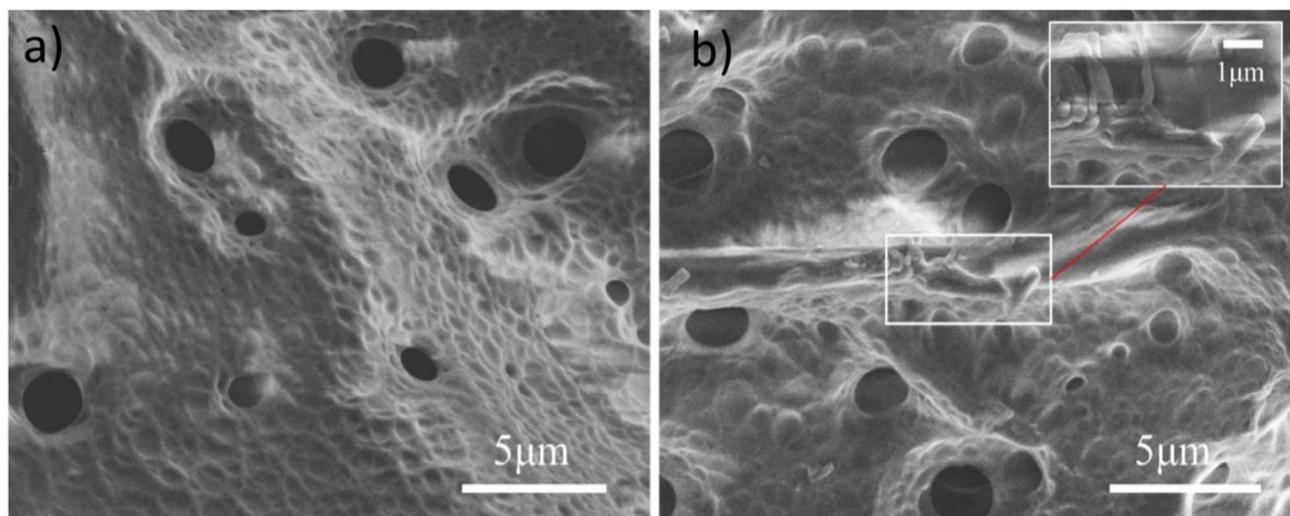Fig. 2   FT-IR spectra of PAA and PAA/DB18C6/GO.

Fig. 1   SEM images of adsorbents. (a) PAA, (b) PAA/DB18C6/GO.

vibration of the aromatic C=C group, which is the main representative peak of the benzene ring. The 1315 cm^{-1} and 860 cm^{-1} peaks are due to the in-plane and out-of-plane bending vibrations of the –CH$_2$ group, respectively. The 1055 cm^{-1} peak is assigned to the symmetric stretching vibration of alicyclic ether C–O–C group.[31,41] These FT-IR results affirm the successful copolymerization of cross-linked PAA hydrogels with dibenzo-18-crown-ether-6 and graphene oxide.

3.1.3 TGA analysis. The thermal stability of the PAA and PAA/DB18C6/GO hydrogel materials were measured in the temperature range of 30–800 °C under nitrogen atmosphere, and the results are presented in Fig. 3. As for PAA and PAA/DB18C6/GO, the process of weight loss can be divided into two main stages. The first stage of weight loss in the temperature range from 30 °C to 400 °C is mainly due to the loss of water molecules in the hydrogel materials, while the second in the range from 400 °C to 800 °C is attributed to the loss of functional groups within the materials and decomposition of the polymer. Compared with PAA, the overall weight loss rate of PAA/DB18C6/GO decreased by 47%, indicating that its thermal stability has improved. This is likely ascribed to the presence of more stable crown-ether and graphene as fillers in the PAA/DB18C6/GO hydrogel composite leading to a reduction in water absorption. Furthermore, there are strong electrostatic interactions and intermolecular hydrogen bonds between the functional groups in the filler and PAA, which enhances the network structure of the hydrogel and thus improves the thermal stability of the material.[35]

3.1.4 Absorbency. The swelling weights of the PAA and PAA/DB18C6/GO hydrogels after immersed in water for 48 h as well as the swelling rates are presented in Table 1. Compared to the pure PAA hydrogel, the swelling rate of 220.75 for PAA/DB18C6/GO is lower, which is ascribed to dibenzo-18-crown-ether-6 and graphene oxide being compounded as support fillers.[23] However, both of the hydrogel composites demonstrate strong water absorption capacity, which significantly promotes the rapid adsorption for Sr^{2+} ions.

3.2 Adsorption performance of adsorbents

For an adsorbent material, a number of parameters such as adsorption equilibrium time, solution pH, adsorbate concentration, environmental temperature and competing ions have been well known to have significant impact on its adsorption performance. Therefore, these parameters were measured under certain conditions in this study to evaluate the adsorption performance of PAA and PAA/DB18C6/GO hydrogel adsorbents below.

3.2.1 Effect of contact time. Adsorption equilibrium time represents adsorption kinetics of adsorbate onto an adsorbent and is thus an important parameter for the adsorbent in practical application. In this study, the adsorption equilibrium time for Sr^{2+} removed by the hydrogel adsorbents was investigated and the obtained results are presented in Fig. 4(a). The adsorption rate of the hydrogel adsorbent is very rapid at the beginning of the process because of the presence of abundant adsorption sites on the surfaces. With increasing adsorption time, the removal rate of strontium ions by PAA/DB18C6/GO increased and reached 85% at about 60 minutes. The adsorption of Sr^{2+} by the hydrogel materials reached equilibrium at 300 min at an initial strontium ion concentration of 280 mg L^{-1}, with the removal rate of 92.83% for PAA and 95.75% for PAA/DB18C6/GO. Compared to PAA, PAA/DB18C6/GO is faster to reach the adsorption equilibrium with a slightly higher removal rate.[25] Therefore, subsequent experiments are performed for 300 min to make sure that the adsorption equilibrium is reached.

3.2.2 Effect of solution pH. The adsorption performance of adsorbents is significantly influenced by the pH of the solution. Additionally, Sr^{2+} exhibit stability under both acidic and alkaline conditions.[60] Therefore, several experiments were performed in this section to investigate the performance of hydrogels in removing Sr^{2+} under different pH conditions. The solution pH was adjusted using 0.1 mol per L sodium hydroxide and/or 0.1 mol per L nitric acid to obtain the desired value. The experimental results are shown in Fig. 4(b). Both PAA and PAA/DB18C6/GO hydrogel materials removed more than 85% of the Sr^{2+} ions in the pH range of 3–10. This is ascribed to dissociation of carboxyl functional groups to a higher degree with increasing pH, leading to generation of a large number of –COO$^-$, which serve as adsorption sites for rapid adsorption of Sr^{2+} *via* electrostatic interaction.[25] The removal rate of Sr^{2+} by PAA/DB18C6/GO hydrogel composite was slightly higher than that by PAA, which was attributed to dibenzo-18-crown-ether-6 and graphene oxide being compounded to increase the adsorption sites for Sr^{2+}.[20] At pH 2, the adsorption capacity of the material is relatively low due to the complete protonation of the carboxyl functional groups of the polymer.[40] On the other
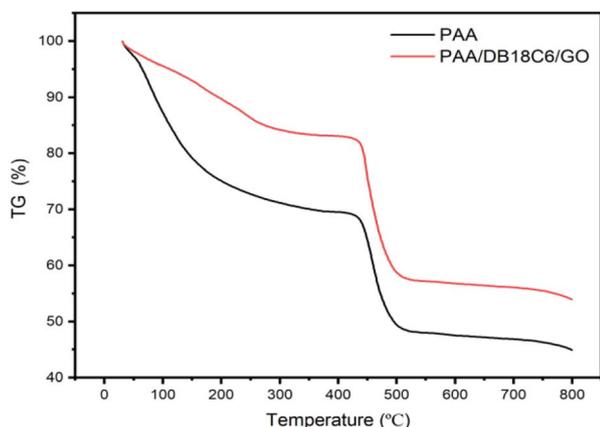

Fig. 3 TGA curves of PAA and PAA/DB18C6/GO.

Table 1 Absorbency parameters of PAA and PAA/DB18C6/GO hydrogels

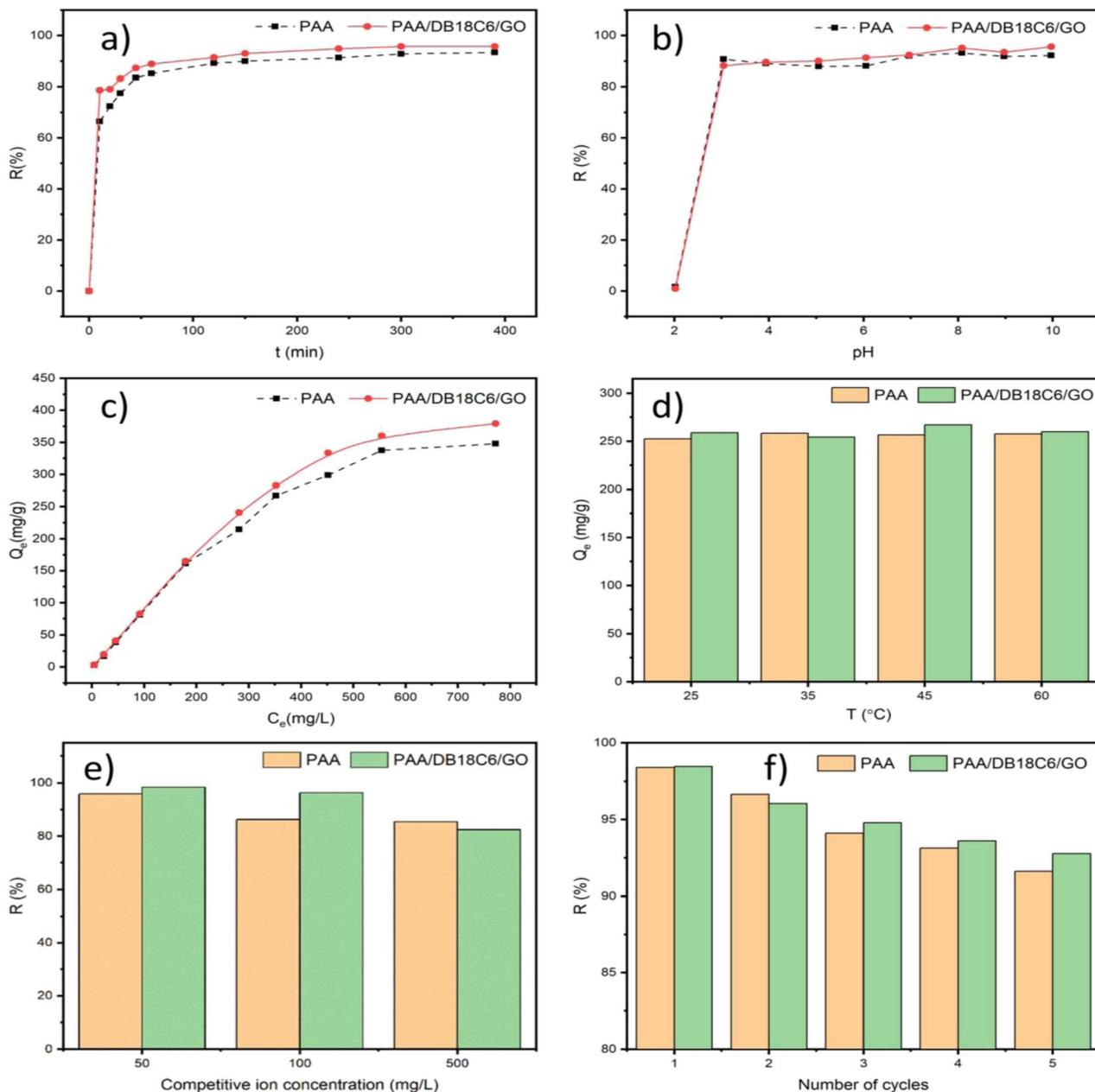| Samples	W_0 (mg)	W_s (mg)	SR
PAA	10.2	3386.5	331.01
PAA/DB18C6/GO	10.1	2239.7	220.75

Fig. 4 The effects of various factors on Sr^{2+} adsorption by α-ZrP and ZrP/18C6. (a) Adsorption time. (b) pH in the solution. (c) Initial Sr^{2+} concentration. (d) Temperature in the solution. (e) Competing ions in solution. (f) Desorption and regeneration.

hand, the adsorption performance of GO for Sr^{2+} is better under alkaline conditions.[61] It is shown that the adsorption performance of PAA/DB18C6/GO hydrogel composite for Sr^{2+} is relatively stable in the pH range of 3 to 10. Therefore, this adsorbent material could have a wide application for treatment of nuclear liquid wastes.

3.2.3 Effect of Sr^{2+} concentration. The adsorption capabilities of PAA and PAA/DB18C6/GO hydrogel composites were investigated at different Sr^{2+} concentrations, and the results are presented in Fig. 4(c). As shown in the figure, the equilibrium adsorption capacities of PAA and PAA/DB18C6/GO for Sr^{2+} are similar at the initial Sr^{2+} concentrations less than 200 mg L^{-1}. However, when the initial Sr^{2+} concentration is higher than

200 mg L^{-1}, the rise in equilibrium adsorption capacity of PAA/DB18C6/GO with increasing Sr^{2+} concentration is more than that of PAA. This is ascribed to higher concentration of strontium ions in the solution increasing the probability of the adsorbent capturing the ions, leading to the increase in adsorption capacity. Furthermore, the unique structure of dibenzo-18-crown-ether-6 is highly selective for Sr^{2+} and thus improve the adsorption efficiency of PAA/DB18C6/GO.[27] Therefore, when the initial concentration of strontium ions in the solution was at 772 mg L^{-1}, the equilibrium adsorption capacities of PAA and PAA/DB18C6/GO for Sr^{2+} were 347.85 mg g^{-1} and 379.35 mg g^{-1}, respectively. As DB18C6 is about 1.5% (in weight) of PAA in the composite, the equilibrium adsorption

Table 2 Comparison of adsorption capacity of PAA/DB18C6/GO hydrogel for Sr^{2+} with other adsorbents

Adsorbents	Initial Sr^{2+} concentration (mg L^{-1})	Contact time (h)	Initial pH	Maximum adsorption capacity (mg g^{-1})	Reference
Natural zeolite	10	48	7.9	1.3	16
Amorphous sodium titanates	438.6	96	7	193.93	42
ZrP/18C6	380	6	7	195.74	43
Polyvinyl alcohol–sulfosuccinic acid	200	6	6.0	60.7	44
P(vinylsulphonic acid/2-acryloamido-2-methyl-1-propanesulphonic acid/magnetic nanoparticles)-carboxymethylcellulose	400	24	6	330	45
Poly(acrylonitrile–butadiene–styrene)	400	1	7	177	46
Hydroxyapatite/poly(acrylamide–acrylic acid)	50	1	6	53.59	47
Acrylic acid/charcoal/montmorillonite	100	48	9.8	26.68	48
Methacrylic acid cryogels	100	24	6.0	209	25
Poly(N-vinyl imidazole-cl-ethylene glycol dimethacrylate)	1000	1	7.0	240.96	49
PAA	772	5	7	347.85	This study
PAA/DB18C6/GO	772	5	7	379.35	This study

capacity of the PAA/DB18C6/GO composite for Sr^{2+} higher than the PAA by 1.5% is significant. Our study[66] shows that the maximum equilibrium adsorption capacity of GO and GO/DADB18C6 for Sr^{2+} are 21.62 mg g^{-1} and 92.21 mg g^{-1}, respectively when the concentration of Sr^{2+} in the solution was 190 mg L^{-1}. Romanchuk et al.[62] found that the maximum adsorption capacity of Sr^{2+} on GO was 23.83 mg g^{-1}. These results also indicate that addition of DB18C6 in the composite significantly enhances the material's adsorption performance for Sr^{2+}. Table 2 summarizes a number of the Sr^{2+} adsorbents with an attention to compare their adsorption capacities. It is shown that PAA and PAA/DB18C6/GO have higher adsorption capacities than other polyacrylic acid-based hydrogel adsorbents,[39] due to high swelling of PAA and the presence of dibenzo-18-crown-ether-6 and graphene oxide in PAA/DB18C6/GO providing more adsorption sites for Sr^{2+}.

3.2.4 Effect of temperature. The effect of environmental temperature on the adsorption performance of PAA and PAA/DB18C6/GO was investigated in this section and the results are presented in Fig. 4(d). The environmental temperatures were set to 25 °C, 35 °C, 45 °C and 60 °C for the adsorption experiments. The results showed that the adsorption capacities of PAA and PAA/DB18C6/GO for Sr^{2+} enhanced slightly with increase in environmental temperature. It can be concluded that the environmental temperature has no apparent influence on the adsorption performance of PAA and PAA/DB18C6/GO. Therefore, both the hydrogel materials can work at the wide temperatures with excellent adsorption performance.

3.2.5 Effect of competing ions. Nuclear wastes are usually complex and contain a large number of radionuclides and metal ions, which arise from nuclear reactions, operation and system processing. It has been shown that high concentrations of Na^+ and K^+ in the waste stream can affect the adsorption performance of the adsorbent for Sr^{2+}.[50] Therefore, a series of experiments were conducted to investigate the adsorption capabilities of PAA and PAA/DB18C6/GO for Sr^{2+} in the presence of competing ions Na^+ and K^+. In these experiments, the

strontium ion concentration was maintained at 50 mg L^{-1}, and Na^+ and K^+ were set to 50 mg L^{-1}, 100 mg L^{-1} and 500 mg L^{-1}, respectively, to study the effect of Na^+ and K^+ concentrations on adsorption of Sr^{2+} on PAA and PAA/DB18C6/GO adsorbents. The experimental results in Fig. 4(e) show that the removal rate of Sr^{2+} by both PAA and PAA/DB18C6/GO decreased with increasing the Na^+ and K^+ concentrations. This indicates that both Na^+ and K^+ ions can compete with Sr^{2+} to some degree for adsorption onto the polyacrylic acid-based adsorbent materials via electrostatic interaction when present in the solution. As the interaction between divalent Sr^{2+} and carboxylate ions in the adsorption sites is stronger than that between monovalent ions Na^+ and K^+ and the carboxylate ions, although the Na^+ and K^+ concentrations in the solutions were 10 times higher than that of Sr^{2+}, the removal rates of Sr^{2+} by PAA and PAA/DB18C6/GO maintained at high levels with 85.41% and 82.41%, respectively. This indicates that PAA and PAA/DB18C6/GO have significantly higher affinity for Sr^{2+} than for Na^+ and K^+.[47]

3.2.6 Recycling. Recycling performance of an adsorbent should be evaluated for an application in terms of cost and secondary waste generated during the waste treatment. In this series of experiments, EDTA-2Na at a concentration of 0.12 mol L^{-1} was used for desorption experiments and 0.1 mol per L sodium hydroxide was applied to regenerate the desorbed hydrogel composites. The effect of PAA and PAA/DB18C6/GO recycling on Sr^{2+} adsorption is shown in Fig. 4(f). When the desorption and regeneration experiments were repeated, the adsorption capacity started to decrease continuously. After five cycles of regeneration, the removal rate of PAA and PAA/DB18C6/GO for Sr^{2+} are 91.6% and 92.8%, respectively. Therefore, the hydrogel composites with good reusability can be used as economic adsorbent materials for the removal of Sr^{2+} from radioactive wastewater.

3.3 Adsorption mechanism of Sr^{2+} onto PAA/DB18C6/GO

3.3.1 Adsorption kinetics study. Although the adsorption process of an adsorbent is largely governed by a number of
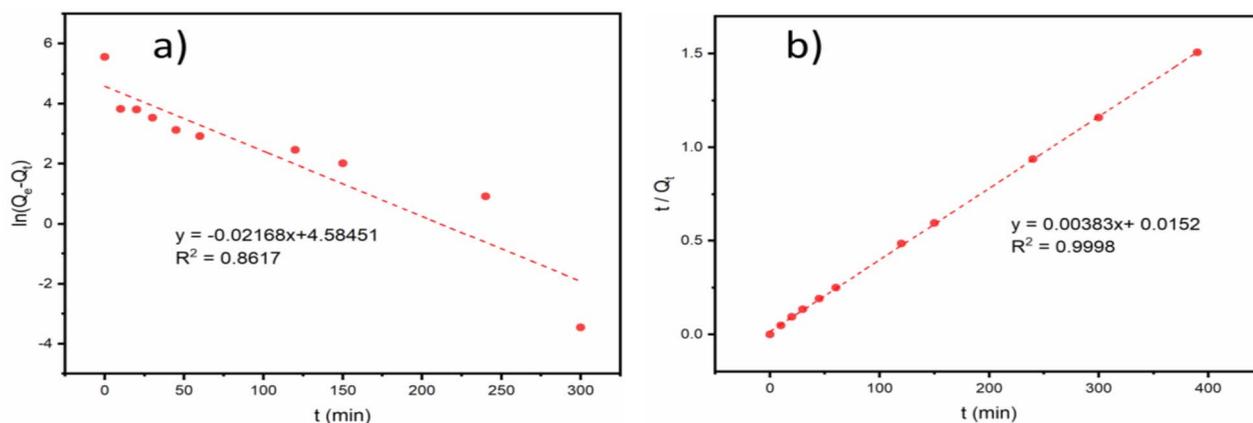
Fig. 5 Kinetic model fitting on Sr^{2+} adsorption by PAA/DB18C6/GO. (a) Pseudo-first order kinetics model. (b) Pseudo-second order kinetics model.

parameters, as studied in Section 3.2, it could fit into the limited adsorption kinetic models. In this study, the experimental data were fitted using the pseudo-first order model[51] and the pseudo-second order model,[52] as presented in eqn (4) and (5), respectively, to deeply investigate the adsorption mechanism of PAA/DB18C6/GO.

$$\ln(Q_e - Q_t) = \ln Q_e - k_1 t \quad (4)$$

$$\frac{t}{Q_t} = \frac{1}{k_2 Q_e^2} + \frac{t}{Q_e} \quad (5)$$

where Q_e (mg g^{-1}) and Q_t (mg g^{-1}) are the adsorption capacity of PAA/DB18C6/GO at adsorption equilibrium and at a certain

adsorption time, respectively; t (min) is the adsorption time; k_1 and k_2 are the adsorption rate constants of the pseudo-first order and the pseudo-second order kinetic models, respectively.

Fig. 5 presents fitting of the adsorption data with the two kinetic models, and the corresponding fitting parameters are listed in Table 3. Compared to the pseudo-first order model, the pseudo-second order kinetic model has a better fit to the adsorption data of Sr^{2+} on PAA/DB18C6/GO with a correlation coefficient of 0.9998. In addition, the theoretical equilibrium adsorption capacity calculated by fitting with the pseudo-second order kinetic model was 261.10 mg g^{-1}, which was closer to the experimental result of 258.85 mg g^{-1}. Therefore, it is desirable that adsorption of Sr^{2+} on PAA/DB18C6/GO

Table 3 Kinetic model fitting parameters of Sr^{2+} adsorption on PAA/DB18C6/GO

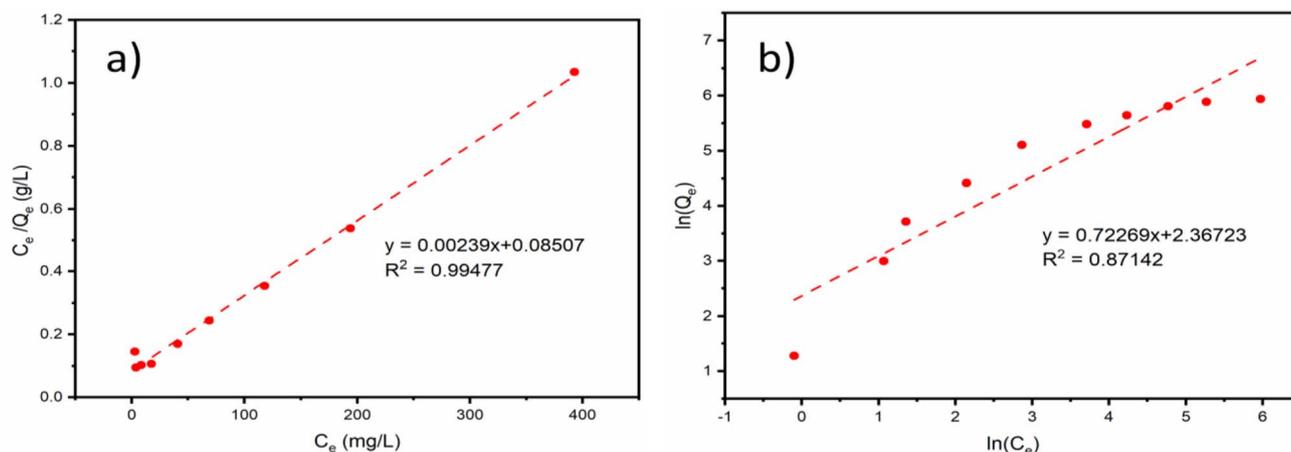| Models	Pseudo-first order			Pseudo-second order		
Modelling parameters	Q_e (mg g^{-1})	k_1 (min^{-1})	R^2	Q_e (mg g^{-1})	k_2 (g min^{-1} mg^{-1})	R^2
Value	97.95	0.0217	0.8617	261.10	0.0010	0.9998

Fig. 6 Thermodynamics isotherm model fitting curves of Sr^{2+} adsorption by PAA/DB18C6/GO. (a) Langmuir adsorption isotherm model. (b) Freundlich adsorption isotherm model.

proceeds with the pseudo-second order model. This implies that chemisorption plays a vital role in the adsorption process.[53,54] The adsorption kinetics of Sr^{2+} by PAA/DB18C6/GO is mainly controlled by the number of the active sites.

3.3.2 Adsorption thermodynamics study. The adsorption isotherm model is typically used to examine the adsorption behavior of an adsorbent. In this study, two adsorption isotherm models: Langmuir[55] and Freundlich[56] were used to analyze the experimental data, as expressed in the following eqn (6) and (7), respectively.

$$\frac{C_e}{Q_e} = \frac{1}{k_L Q_m} + \frac{C_e}{Q_m} \tag{6}$$

$$\ln Q_e = \ln k_F + \frac{1}{n} \ln C_e \tag{7}$$

where, C_e (mg L^{-1}) is the concentration of Sr^{2+} in solution at adsorption equilibrium; Q_e (mg g^{-1}) is the adsorption capacity of the adsorbent at Sr^{2+} adsorption equilibrium; Q_m (mg g^{-1}) is the saturation adsorption capacity of the adsorbent for Sr^{2+}; k_L (L mg^{-1}) and k_F (L mg^{-1}) are the adsorption equilibrium constants of the Langmuir adsorption isotherm model and Freundlich adsorption isotherm model, respectively; n is the heterogeneity factor, which is an adsorption empirical constant related to the adsorption strength.

Fig. 6 presents fitting results of the experimental adsorption data with the above two models. The corresponding model fitting parameters were summarized in Table 4. The fitting results suggest that the experimental data have a better fit to the Langmuir isotherm model than the Freundlich isotherm model due to the higher correlation coefficient of 0.99477. This could be ascribed to more adsorption sites presented on the PAA/DB18C6/GO hydrogel composite surface due to the presence of dibenzo-18-crown-ether-6 and graphene oxide in the PAA hydrogel. Therefore, the adsorption of Sr^{2+} on the PAA/DB18C6/GO composite prefers to proceed with a monolayer adsorption process.[31] Furthermore, the extremely high adsorption capacity of 418.41 mg g^{-1} obtained by fitting indicates that PAA/DB18C6/GO has a remarkable adsorption potential for the removal of Sr^{2+} from the nuclear liquid wastes.

3.3.3 Mechanism study. A schematic of the adsorption mechanism of the PAA/DB18C6/GO composite for Sr^{2+} is presented in Fig. 7. The chemical structures of polyacrylic acid, dibenzo-18-crown-6 and graphene oxide are presented on top of the figure to clearly exhibit the functional groups of each component. PAA contains a large number of carboxyl groups which can interact with strontium ions through electrostatic interaction, coordination complex and hydrogen bonding.[40,67,68] GO contains many oxygen-containing groups, including carboxyl and hydroxyl groups at the base and edges, which have

Table 4 Isotherm model fitting parameters of Sr^{2+} adsorption by PAA/DB18C6/GO

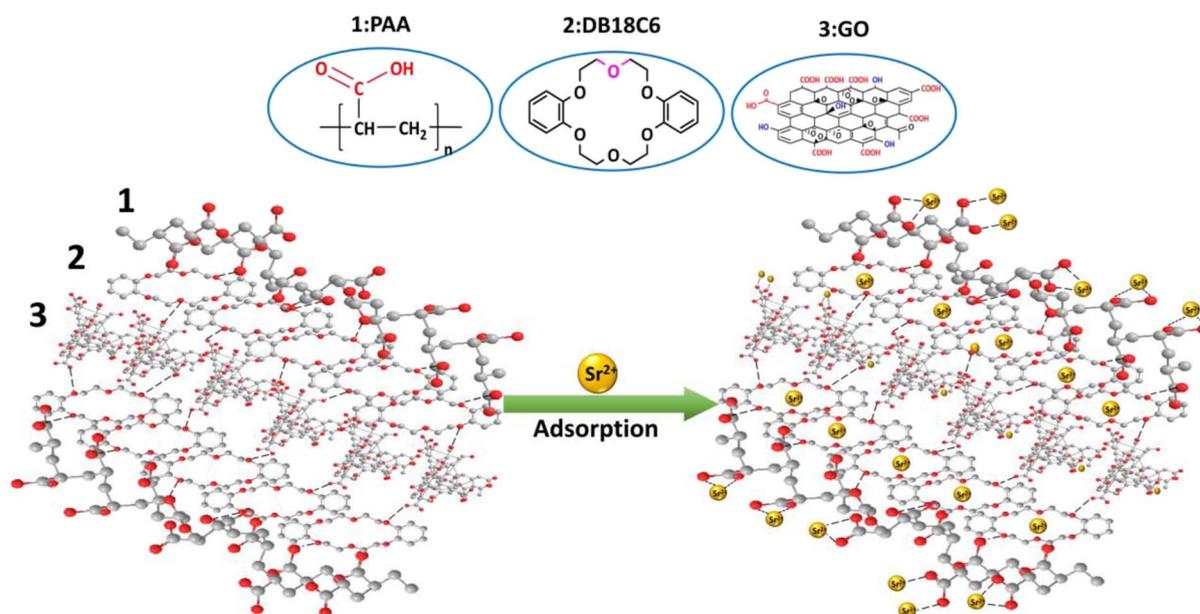| Models	Langmuir			Freundlich		
Modelling parameters	Q_m (mg g^{-1})	k_L (L mg^{-1})	R^2	$1/n$	k_F [(mg g^{-1}) (L mg^{-1})$^{1/n}$]	R^2
Value	418.41	0.0281	0.99477	0.7227	10.6678	0.87142

Fig. 7 Schematic chemical structures of polyacrylic acid, dibenzo-18-crown-6 and graphene oxide and adsorption mechanism diagrams for Sr^{2+}.
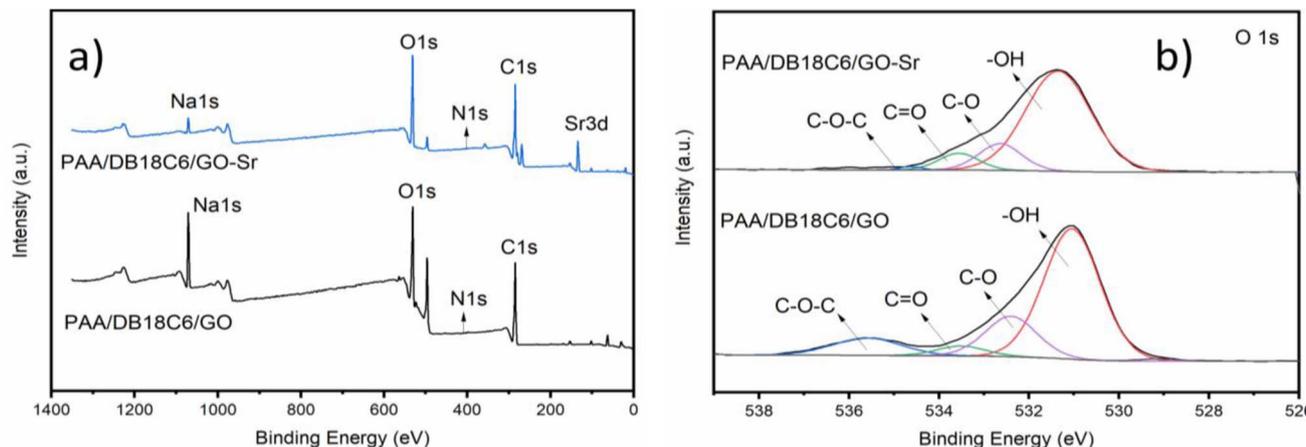
Fig. 8 XPS spectra of PAA/DB18C6/GO before and after Sr^{2+} adsorption. (a) Full scan spectrum. (b) O 1s.

strong adsorption properties for the metal ions.[63–65] The unique heterocyclic structure of DB18C6 exhibits a high selectivity for Sr^{2+}. To further investigate the adsorption mechanism of Sr^{2+} onto the PAA/DB18C6/GO hydrogel composite, the adsorbent before and after Sr^{2+} adsorption was characterized using XPS, as shown in Fig. 8(a). The XPS spectrum of the PAA/DB18C6/GO material shows a distinct Sr 3d peak at 133.78 eV after Sr^{2+} adsorption,[57] which was not observed before the adsorption. This indicates that the Sr^{2+} ions have been adsorbed onto PAA/DB18C6/GO. In addition, the Na 1s peak located at 1071.32 eV can be seen obviously,[42] and its intensity is significantly reduced after Sr^{2+} adsorption. It is inferred that the sodium ions in PAA/DB18C6/GO were released from the material due to the sodium ions being exchanged out for the strontium ions during the adsorption process.[17,42] The O 1s peak in the PAA/DB18C6/GO material before and after Sr^{2+} adsorption was analyzed by the Gauss–Lorentz method. Fig. 8(b) shows that the O 1s peak is deconvoluted to four peaks located at 531.04 eV, 532.40 eV, 533.51 eV and 535.60 eV, respectively, which are assigned to –OH, C–O, C=O and C–O–C, respectively.[58] Compared to the deconvoluted O 1s in the raw material, the intensity of the C–O–C peak in the adsorbed material is significantly weaker. This suggests that the crown ether is involved in the adsorption process, leading to higher adsorption capacity for the PAA/DB18C6/GO hydrogel, compared to the PAA.[20,59]

4 Conclusions

In this work, the novel PAA/DB18C6/GO hydrogel composite was successfully prepared by free radical cross-linking copolymerization method and its adsorption properties were investigated in details to evaluate the application in treating nuclear wastes. The results show that the PAA/DB18C6/GO adsorbent has an extremely high adsorption capacity with 379.35 mg g^{-1} at the initial Sr^{2+} concentration of 772 mg L^{-1}, compared to the PAA hydrogel, due to the unique structure of dibenzo-18-crown-ether-6 and high swelling. The removal rate of Sr^{2+} by PAA/DB18C6/GO was kept at a relatively high value of 85% within 60 min at an initial Sr^{2+} concentration of 300 mg L^{-1}. The PAA/

DB18C6/GO constantly maintains remarkable adsorption performance in the wide solution pH range of 3–10 and the temperature range of 25–60 °C. The composite shows a high affinity for strontium ions with a removal rate of 82.4% when the concentrations of competing ions Na^+ and K^+ in the solution were 10 times higher than that of Sr^{2+}. The PAA/DB18C6/GO demonstrates good reusability after five continuous desorption and regeneration cycles as removal rate of more than 92% for Sr^{2+} was maintained. Analyses on the experimental data reveal that the adsorption of Sr^{2+} onto PAA/DB18C6/GO is mainly dominated by chemisorption *via* monolayer mode. Consequently, PAA/DB18C6/GO is a promising candidate for the removal of strontium ions from liquid wastes under wide environmental conditions.

Author contributions

Sheng Chen: conceptualization, investigation; Lina Wu: investigation, writing – original draft; Zhicheng Wu: data curation, formal analysis, writing – review & editing; Zhikun Liu: methodology, investigation; Zhihua Qiu: project administration, resources; Lisheng Chi: funding acquisition, supervision. All authors have given approval to the final version of the manuscript.

Conflicts of interest

The authors declare that they have no competing interests.

Acknowledgements

Notes and references

1 M. T. Majeed, T. Luni and T. Tahir, *Environ. Sci. Pollut. Res.*, 2022, **29**, 61107–61121.

2   M. Sadiq, F. Wen, M. F. Bashir and A. Amin, *J. Cleaner Prod.*, 2022, **375**, 133965.

3   A. A. Syed, M. A. Kamal and R. Tripathi, *Environ. Sci. Pollut. Res.*, 2021, **28**, 54744–54755.

4   S. K. Sahoo, N. Kavasi, A. Sorimachi, H. Arae, S. Tokonami, J. W. Mietelski, E. Łokas and S. Yoshida, *Sci. Rep.*, 2016, **6**, 23925.

5   R. Behrens, *J. Instrum.*, 2020, **15**, P05015.

6   A. Burger and I. Lichtscheidl, *Sci. Total Environ.*, 2019, **653**, 1458–1512.

7   S. Pors Nielsen, *Bone*, 2004, **35**, 583–588.

8   Y. Guo, N. T. Hong Nhung, X. Dai, C. He, Y. Wang, Y. Wei and T. Fujita, *Front. Bioeng. Biotechnol.*, 2022, **10**, 819407.

9   P. N. Khan, A. Bhattacharyya, J. N. Sharma and S. Manohar, *J. Hazard. Mater.*, 2020, **397**, 122476.

10 C. Wang, D. Chang, Y. Shen, Y. Sun and C. Wu, *J. Sep. Sci.*, 2017, **40**, 3866–3872.

11 Y. K. Kim, S. Kim, Y. Kim, K. Bae, D. Harbottle and J. W. Lee, *Appl. Surf. Sci.*, 2019, **493**, 165–176.

12 R. K. Vishwakarma, P. K. Narayanam, R. Umamaheswari and K. Sundararajan, *J. Environ. Manage.*, 2021, **298**, 113443.

13 S. İnan, *J. Radioanal. Nucl. Chem.*, 2022, **331**, 1137–1154.

14 D. Alby, C. Charnay, M. Heran, B. Prelot and J. Zajac, *J. Hazard. Mater.*, 2018, **344**, 511–530.

15 S. Singh, D. Kapoor, S. Khasnabis, J. Singh and P. C. Ramamurthy, *Environ. Chem. Lett.*, 2021, **19**, 2351–2381.

16 T. Abdollahi, J. Towfighi and H. Rezaei-Vahidian, *Environ. Technol. Innovation*, 2020, **17**, 100592.

17 R. Yi, G. Ye and J. Chen, *RSC Adv.*, 2019, **9**, 27242–27249.

18 H. Li, Y. Huang, J. Liu and H. Duan, *Chemosphere*, 2021, **282**, 131046.

19 K. Gupta, B. Yuan, C. Chen, N. Varnakavi and M.-L. Fu, *Chem. Eng. J.*, 2019, **369**, 803–812.

20 C. Guo, M. Yuan, L. He, L. Cheng, X. Wang, N. Shen, F. Ma, G. Huang and S. Wang, *CrystEngComm*, 2021, **23**, 3349–3355.

21 Md. A. Momen and M. L. Dietz, *React. Funct. Polym.*, 2021, **160**, 104829.

22 C. Özeroğlu and G. Keçeli, *J. Radioanal. Nucl. Chem.*, 2006, **268**, 211–219.

23 Y. Tang, H. Tang, F. Wang, C. Guan and L. Zhu, *Polym. Sci., Ser. B*, 2019, **61**, 471–478.

24 Q. Lv, X. Hu, X. Zhang, L. Huang, Z. Liu and G. Sun, *Mater. Des.*, 2019, **181**, 107934.

25 A. Baimenov, F. Montagnaro, V. J. Inglezakis and M. Balsamo, *Ind. Eng. Chem. Res.*, 2022, **61**, 8204–8219.

26 P. Mohammadzadeh Pakdel and S. J. Peighambardoust, *J. Environ. Manage.*, 2018, **217**, 123–143.

27 N. A. Bezhin and I. I. Dovhyi, *Russ. Chem. Rev.*, 2015, **84**, 1279–1293.

28 J. W. Steed, *Coord. Chem. Rev.*, 2001, **215**, 171–221.

29 Md. R. Awual, T. Yaita, T. Taguchi, H. Shiwaku, S. Suzuki and Y. Okamoto, *J. Hazard. Mater.*, 2014, **278**, 227–235.

30 E. P. Horwitz, M. L. Dietz and D. E. Fisher, *Solvent Extr. Ion Exch.*, 1990, **8**, 199–208.

31 H.-R. Yu, J.-Q. Hu, Z. Liu, X.-J. Ju, R. Xie, W. Wang and L.-Y. Chu, *J. Hazard. Mater.*, 2017, **323**, 632–640.

32 A. Y. Romanchuk, A. S. Kuzenkova, A. S. Slesarev, J. M. Tour and S. N. Kalmykov, *Solvent Extr. Ion Exch.*, 2016, **34**, 594–602.

33 M. Hasanpour and M. Hatami, *Adv. Colloid Interface Sci.*, 2020, **284**, 102247.

34 S. D. Sarkar, Md. M. Uddin, C. K. Roy, Md. J. Hossen, M. I. Sujan and Md. S. Azam, *RSC Adv.*, 2020, **10**, 10949–10958.

35 M. A. Awad and L. S. Jasim Al-Hayder, *IOP Conf. Ser.: Mater. Sci. Eng.*, 2020, **928**, 052033.

36 F. Ganji, S. Vasheghani-Farahani and E. Vasheghani-Farahani, *Iran. Polym. J.*, 2010, **19**, 375–398.

37 G. Sennakesavan, M. Mostakhdemin, L. K. Dkhar, A. Seyfoddin and S. J. Fatihhi, *Polym. Degrad. Stab.*, 2020, **180**, 109308.

38 L. Guan, H. Kang, W. Liu and D. Tian, *Int. J. Biol. Macromol.*, 2021, **177**, 48–57.

39 C. Özeroğlu and Ö. D. Bilgiç, *J. Radioanal. Nucl. Chem.*, 2015, **305**, 551–565.

40 L. J. Kirwan, P. D. Fawell and W. van Bronswijk, *Langmuir*, 2003, **19**, 5802–5807.

41 X. Zheng, S. Song, J. Yang, J. Wang and L. Wang, *Eur. Polym. J.*, 2019, **112**, 581–590.

42 G. Kim, D. S. Lee, H. Eccles, S. M. Kim, H. U. Cho and J. M. Park, *RSC Adv.*, 2022, **12**, 18936–18944.

43 L. Wu, H. Wang, X. Kong, H. Wei, S. Chen and L. Chi, *RSC Adv.*, 2023, **13**, 6346–6355.

44 J. Y. Yoon, H. Zhang, Y. K. Kim, D. Harbottle and J. W. Lee, *J. Environ. Chem. Eng.*, 2019, **7**, 102824.

45 A. M. Emara, F. H. El-Sweify, S. F. Abo-Zahra, A. I. Hashim and T. E. Siyam, *Radiochim. Acta*, 2019, **107**, 695–711.

46 M. I. Aly, M. R. Hassan, M. M. Ghobashy and B. A. Masry, *Part. Sci. Technol.*, 2021, **40**, 697–711.

47 H. S. Hassan, A. M. El-Kamash and H. A.-S. Ibrahim, *Environ. Sci. Pollut. Res.*, 2019, **26**, 25641–25655.

48 N. A. A. Reheim, M. A. Geleel, A. A. Mohammed, E. R. Atta, E. A. Elsawy and A. Tawfik, *J. Radioanal. Nucl. Chem.*, 2019, **322**, 455–465.

49 G. Garg, G. S. Chauhan and J. h. Ahn, *J. Appl. Polym. Sci.*, 2011, **124**, 3721–3727.

50 S. Eun, J. Ryu, H. Kim, H.-J. Hong and S. Kim, *J. Environ. Manage.*, 2021, **297**, 113389.

51 H. Yuh-Shan, *Scientometrics*, 2004, **59**, 171–177.

52 Y. S. Ho and G. McKay, *Process Biochem.*, 1999, **34**, 451–465.

53 F.-C. Wu, R.-L. Tseng and R.-S. Juang, *Chem. Eng. J.*, 2009, **153**, 1–8.

54 Y. S. Ho and G. McKay, *Process Saf. Environ. Prot.*, 1998, **76**, 332–340.

55 I. Langmuir, *J. Am. Chem. Soc.*, 1916, **38**, 2221–2295.

56 H. Freundlich, *Z. Phys. Chem., Stoechiom. Verwandtschaftsl.*, 1906, **57**, 385–470.

57 Z. Jiao, Y. Meng, C. He, X. Yin, X. Wang and Y. Wei, *Microporous Mesoporous Mater.*, 2021, **318**, 111016.

58 J.-C. Dupin, D. Gonbeau, P. Vinatier and A. Levasseur, *Phys. Chem. Chem. Phys.*, 2000, **2**, 1319–1324.

59 L. Zhu, Y. Liu, Y. Liu and Y. Tang, *Polym. Polym. Compos.*, 2022, **30**, 1–14.

60 J. Wang, *Inorganic Chemistry*, Higher Education Press, 2018.

61 C. Ding, W. Cheng, Y. Sun and X. Wang, *Dalton Trans.*, 2014, **43**, 3888–3896.

62 A. Y. Romanchuk, A. S. Slesarev, S. N. Kalmykov, D. V. Kosynkin and J. M. Tour, *Phys. Chem. Chem. Phys.*, 2013, **15**, 2321.

63 X. Wang, Z. Chen and X. Wang, *Sci. China Chem.*, 2015, **58**, 1766–1773.

64 W. Peng, H. Li, Y. Liu and S. Song, *J. Mol. Liq.*, 2017, **230**, 496–504.

65 M. M. Velásquez-Rojas, F. F. Contreras-Torres, V. Meza-Laguna, E. Álvarez-Zauco, M. H. Farías, V. A. Basiuk and E. V. Basiuk, *Mater. Chem. Phys.*, 2021, **260**, 124127.

66 L. Wu, Master Degree Dissertation, Fuzhou University, 2023.

67 M. Bubeníková, P. Ecorchard, L. Szatmáry, O. Mrózek, P. Salačová and J. Tolasz, *J. Radioanal. Nucl. Chem.*, 2018, **315**, 263–272.

68 V. Neßlinger, A. G. Orive, D. Meinderink and G. Grundmeier, *J. Colloid Interface Sci.*, 2022, **615**, 563–576.

69 W. Liu, L. Yang, M. Yu and M. Liu, *Chin. J. Anal. Chem.*, 2016, **44**, 707–715.

70 N. Rahimi, D. G. Molin, T. J. Cleij, M. A. van Zandvoort and M. J. Post, *Biomacromolecules*, 2012, **13**, 1448–1457.